Wideband Array Signal Processing Using MCMC Methods

William Ng, James P. Reilly*, Thia Kirubarajan, and Jean-René Larocque
Department of Electrical and Computer Engineering,
McMaster University, 1280 Main St. W.,
Hamilton, Ontario,
Canada L8S 4K1

Abstract

This paper proposes a novel wideband structure for array signal processing. A new interpolation model is formed where the observations are linear functions of the source amplitudes, but nonlinear in the direction of arrival (DOA) parameters. The interpolation model also applies to the narrowband case. The proposed method lends itself well to a Bayesian approach for jointly estimating the model order and the DOAs through a reversible jump Markov chain Monte Carlo (MCMC) procedure. The source amplitudes are estimated through a *maximum a posteriori* (MAP) process. Advantages of the proposed method include joint detection of model order and estimation of the DOA parameters, the fact that reliable performance can be obtained using significantly fewer observations than previous wideband methods, and that only real arithmetic is required. The DOA estimation performance of the proposed method is compared with the theoretical Cramer Rao lower bound (CRLB) for this problem. Simulation results demonstrate the effectiveness and robustness of the method.

I. Introduction

Array signal processing, a mature and specialized branch of signal processing, has found use in radar, sonar, communications, geophysical exploration, astrophysical exploration, biomedical signal processing, and acoustics [1] [2]. It focuses on extracting as much information as possible from an environment using an array of independent sensors. These sensors are placed at different points in space to "listen" to the received signal. In effect, the sensors provide a means of sampling the received signal in space.

Array signal processing has to do with 1) detecting the number of incident sources (model order), 2) estimating parameters, like direction-of-arrival (DOA) or inter-sensor delay (ISD) of the sources impinging onto the array, and 3) recovering the incident source waveforms. Methods for each of the above objectives can be classified as either narrowband or wideband. For the narrowband scenario, there exist many algorithms to solve the estimation problem [1] [3] [4] [5] [6] [7]. Methods such as [4] [5] can perform determination of model order and the estimation

Permission to publish abstract separately is granted.
J. Reilly, corresponding author: ph: 905 525 9140 x22895, fax: 905 521 2922, email: reillyj@mcmaster.ca

of desired signal parameters jointly rather than independently. On the other hand, for the wideband scenario, it appears there is no existing method which can attain the objective of joint detection and estimation simultaneously.

A common approach to wideband signal processing is to sample the spectrum of the incoming signals at each sensor to form an array of narrowband signals. In the so-called *incoherent signal-subspace processing* method [8], the narrowband signals at each frequency are processed separately, and the results from all frequency bins are combined to obtain the final result. However, the performance of this approach [9] [10] degrades when the sources are correlated and the SNR is low. An alternative approach in [11] [12] uses the *coherent signal-subspace method* (CSM) that utilizes the so-called *focusing* technique to transform the correlation matrix of the observations at different frequency bins to a common subspace. Having done that, algorithms developed for narrowband models can be used to solve wideband signal processing problems. For example, well-established methods like the Akaike information criterion (AIC) and the minimum description length (MDL) algorithm [13] can be used to detect the number of sources, and high resolution algorithms like the MUSIC [3] can then be used to estimate the DOAs.

An alternative focusing approach has been developed in [9] [10], but suffers from the asymptotic bias of the peaks in the spatial spectrum. This bias increases with the bandwidth of the sources and the deviation of the focusing points from the true DOAs. A similar approach that uses a two-sided unitary transformation on the correlation matrices (TCT) in different frequency bins was introduced [9] [10] [14]. This approach reduces the error of the subspace fitting and removes the bias of the estimation found in CSM. Like other approaches, TCT requires a lot of observations to compute the correlation matrices corresponding to different frequency bins. Furthermore, recovery of the source amplitudes can be expensive with focusing techniques, since the narrowband source waveforms must be calculated at each frequency bin, and then combined through an FFT to yield the final wideband source estimate. Other wideband methods appear in [15] and [16].

Previously, separate models and analysis methods were required for the narrowband and wideband scenarios. In this paper, a novel model structure which applies equally well to both these cases is proposed, that detects model order, estimates DOA, and recovers the source waveforms in a computationally efficient manner. Markov chain Monte Carlo (MCMC) [4] [17] [18] [19] methods are well suited for extraction of the parameters of interest associated with this model. MCMC methods are Bayesian techniques based on the idea of numerically sampling posterior distributions of interest that are difficult or impossible to handle analytically [19]. The approach proposed in this paper is an extension of the method of [4] to seamlessly perform joint detection of the number of sources and estimation of ISDs (DOAs), and recovery of the sources, for both narrowband and wideband models.

The proposed approach offers the functionality of wideband beamforming [1] [2], as well as wideband DOA estimation and detection. The proposed algorithm can be used in a beamforming

context because it recovers the source signals which are mixed at the sensor outputs. The proposed method is somewhat more computationally expensive than previous wideband methods (e.g., [10]) which estimate the DOAs only. However, in cases when the model order, the DOAs, and the source waveforms are all required, then the proposed method shows a comparable computational expense relative to the other methods.

There are several advantages offered by this approach in array signal processing. Firstly, by virtue of the *reversible jump Metropolis-Hastings algorithm* [20], the proposed MCMC approach *jointly* detects the model order and estimates all parameters of interest for both wideband and narrowband scenarios. This procedure is more efficient and accurate than other common approaches that would perform each process independently. Secondly, unlike other approaches, like CSM and TCT, the proposed approach requires far fewer observations for processing, because the correlation matrix of the observations is not explicitly required. Thirdly, the method benefits from requiring only real arithmetic, in contrast to previous methods which require complex arithmetic. This fact results in significant reductions in hardware complexity, since the need for quadrature mixing to IF frequencies is alleviated. Also, like other wideband methods, the sources can be partially or fully correlated.

This paper is organized as follows. Section II presents a general model based on interpolation techniques to represent wideband signals. This model includes narrowband signals (with small but finite bandwidth) without modification. Section III describes the derivation of the necessary probability distributions. A description of the reversible jump MCMC algorithm used for model order detection is given in Section IV, followed by the simulation results and discussion in Section V. Conclusions are given in Section VI.

Notation: Bold upper case symbols denote matrices, bold lower case symbols denote vectors. The superscript ^{T} denotes the transpose operation, and the symbol "$\sim$" means "distributed as." The quantity $p(\cdot)$ denotes a prior probability distribution, $l(\cdot)$ denotes a likelihood, and $\pi(\cdot)$ denotes a posterior distribution.

II. The Data Model

A. One-dimensional Model

A uniform linear array with M elements is assumed.[1] For the time being, assume further that 1) we are operating in a noiseless environment, 2) only a single source $s(t)$ is incident onto the array, where the source $s(t)$ may be a wideband signal, whose frequency response is band limited to

$$|f| \in \left[f^l, f^u\right], \quad f^u = f^l + \Delta f, \tag{1}$$

[1]For ease of presentation, we consider the uniform linear array case. However, the method can be extended to arbitrary linear geometries. Planar geometries can also be considered, provided the sources and all elements of the array are in the same plane.

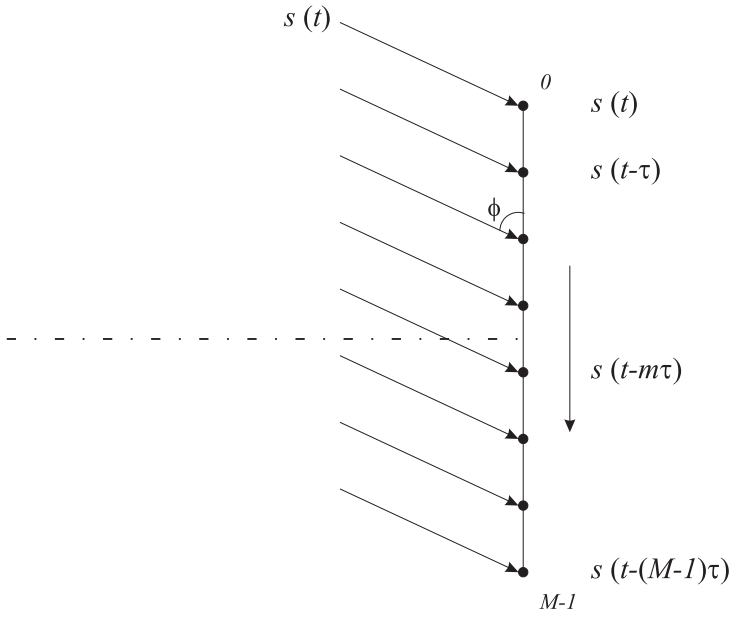

Fig. 1. A signal $s(t)$ impinging onto the array when the incident angle ϕ is less than $\pi/2$ with respect to the 0th sensor.

where f^l and f^u are the lower and upper frequencies, and Δf is the bandwidth of the signal, and 3) the signal $s(t)$ impinges onto the array at an angle ϕ less than $\pi/2$ with respect to the axis of the array, as illustrated in Fig. 1. The incident signals are assumed to have finite bandwidth. The signal $s(t)$ is discretized at some suitable sampling interval to yield the discrete sequence $s(n)$. In this noise-free case, we can approximate the mth sensor output as follows

$$s(t - m\tau) \approx \sum_{l=0}^{L-1} h_l(m\tau)s(n - l), \quad m = 0, \ldots, M - 1, \tag{2}$$

where τ, the inter-sensor delay (ISD), is defined as [1]

$$\tau \triangleq \frac{\Delta}{C} \sin \phi, \tag{3}$$

where Δ is the interspacing of the sensors and C is the speed of propagation. The quantity $h_l(m\tau)$ is the lth sample of an interpolating sequence $\{h_l(m\tau), l = 0, ..., L - 1\}$.[2] Using the fact that

$$\Delta \leq \frac{1}{2}\lambda_{min} = \frac{C}{2f_{max}}, \tag{4}$$

where f_{max} is the maximum possible frequency component of the incident wave, we can write

$$\frac{\Delta}{C} \leq \frac{1}{2f_{max}}. \tag{5}$$

Comparing (5) to (3), we have

$$|\tau| \leq \frac{1}{2f_{max}} = \frac{1}{2f^u} \triangleq T_{max}. \tag{6}$$

[2]For example, in the case of the uniform linear array, the interpolation sequence can be a windowed $sinc(\cdot)$ function.

Therefore, we have $\tau \in [-T_{max}, T_{max}]$.

We can express the received signal vector $\boldsymbol{s}(t) = [s(t), s(t-\tau), \ldots, s(t-(M-1)\tau)]^T$ in (2) for $m = 0, 1, ..., M-1$ in vector form as follows

$$\begin{bmatrix} s(t) \\ s(t-\tau) \\ \vdots \\ s(t-(M-1)\tau) \end{bmatrix} \approx \begin{bmatrix} h_0(0) & h_1(0) & \ldots & h_{L-1}(0) \\ h_0(\tau) & h_1(\tau) & \ldots & h_{L-1}(\tau) \\ \vdots & \vdots & \ddots & \vdots \\ h_0((M-1)\tau) & h_1((M-1)\tau) & \ldots & h_{L-1}((M-1)\tau) \end{bmatrix} \begin{bmatrix} s(n) \\ s(n-1) \\ \vdots \\ s(n-L+1) \end{bmatrix} \tag{7}$$

which can be written as

$$\boldsymbol{s}(t) = \boldsymbol{H}(\tau)\boldsymbol{s}(n), \tag{8}$$

where[3] $\boldsymbol{s}(n)$ is known as the signal vector

$$\boldsymbol{s}(n) \quad = \quad [s(n), s(n-1), \ldots, s(n-L+1)]^T, \tag{9}$$

and $\boldsymbol{H}(\tau) \in \mathcal{R}^{M \times L}$ is an *interpolation matrix* for τ and is defined in terms of L column vectors as

$$\boldsymbol{H}(\tau) \triangleq [\boldsymbol{h}_0(\tau), \boldsymbol{h}_1(\tau), \ldots, \boldsymbol{h}_{L-1}(\tau)], \tag{10}$$

where $\boldsymbol{h}_l(\tau) \in \mathcal{R}^{M \times 1}$ is the lth column of the interpolation matrix $\boldsymbol{H}(\tau)$, defined as

$$\boldsymbol{h}_l(\tau) \triangleq [h_l(0), h_l(\tau), \ldots, h_l((M-1)\tau)]^T. \tag{11}$$

Accordingly, we can rewrite the sensor output vector in the form

$$\boldsymbol{s}(t) = \boldsymbol{h}_0(\tau)s(n) + \sum_{l=1}^{L-1} \boldsymbol{h}_l(\tau)s(n-l). \tag{12}$$

Thus the sensor output can be expressed as a linear combination of a set of L vectors of $\{\boldsymbol{h}_l(\tau), l = 0, 1, ..., L-1\}$ with the signals $\boldsymbol{s}(n)$ as the associated coefficients.

In cases where the incident angle ϕ of a signal $s(t)$ is greater than $\pi/2$ with respect to the 0th sensor, as illustrated in Fig. 2, the $(M-1)$th sensor becomes the first sensor that receives $s(t)$, while the 0th sensor will not receive the signal until $(M-1)\tau$ seconds later. Following the same development of (2), we may express the pth sensor output for $\phi > \pi/2$ in the following manner

$$s(t-p\tau) = \sum_{l=0}^{L-1} h_l(p\tau)s(n-l), \tag{13}$$

where $p = M-1-m$. Extending the above for all $p = M-1, M-2, ..., 0$, we can write

$$\boldsymbol{s}(t) = \boldsymbol{E}_M \boldsymbol{H}(\tau)\boldsymbol{s}(n), \tag{14}$$

[3]Note that for notational convenience, from this point onwards we replace the approximation with an equality.

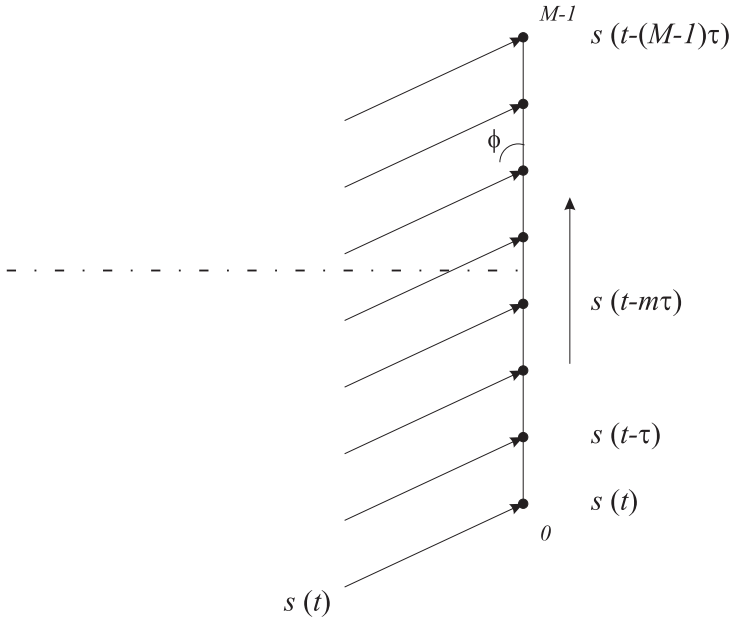

Fig. 2. A signal $s(t)$ impinging onto the array when the incident angle ϕ is greater than $\pi/2$ with respect to the 0th sensor.

where $\boldsymbol{E}_M \in \mathcal{R}^{M\times M}$ is a *exchange matrix* defined as follows [21]

$$\boldsymbol{E}_M = \begin{bmatrix} 0 & 0 & \dots & 1 \\ 0 & \dots & 1 & 0 \\ \vdots & \ddots & \ddots & \vdots \\ 1 & 0 & 0 & 0 \end{bmatrix}. \tag{15}$$

In other words, if the incident angle ϕ of a signal is greater than $\pi/2$ with respect to the 0th sensor, the expression of the sensor output vector is the same as that defined in (8) pre-multiplied by the exchange matrix $\boldsymbol{E}_M$ that reverses the order of rows in the interpolation matrix $\boldsymbol{H}(\tau)$. Therefore, the general expression for a sensor output vector in response to an incoming signal $s(t)$ at an angle ϕ is

$$\boldsymbol{s}(t) = \tilde{\boldsymbol{H}}(\tau)\boldsymbol{s}(n) = \tilde{\boldsymbol{h}}_0(\tau)s(n) + \sum_{l=1}^{L-1} \tilde{\boldsymbol{h}}_l(\tau)s(n-l) \tag{16}$$

where

$$\tilde{\boldsymbol{H}}(\tau) = \begin{cases} \boldsymbol{H}(\tau), & \text{if} \quad \phi \le \pi/2 \\ \boldsymbol{E}_M\boldsymbol{H}(\tau), & \text{if} \quad \phi > \pi/2 \end{cases}, \qquad \text{where } \tilde{\boldsymbol{H}}(\tau) \in \mathcal{R}^{M\times L}. \tag{17}$$

An analogous definition holds for the vector $\tilde{\boldsymbol{h}}_l(\tau)$.

B. The K-dimensional Model

The model above can be easily extended to cases where there exist multiple sources $K \ge 1$. The incident angle and delay parameters now become vectors, i.e., $\boldsymbol{\phi}$ and $\boldsymbol{\tau}$, respectively. They

are defined as

$$\boldsymbol{\phi} = [\phi_0, \phi_1, \ldots, \phi_{K-1}]^T, \tag{18}$$

$$\boldsymbol{\tau} = [\tau_0, \tau_1, \ldots, \tau_{K-1}]^T. \tag{19}$$

To extend the model described earlier to the K-dimensional case, we need to add a subscript k to τ and $s(t)$ such that (16) becomes

$$\boldsymbol{s}_k(t) = \tilde{\boldsymbol{H}}(\tau_k)\boldsymbol{s}_k(n) = \tilde{\boldsymbol{h}}_0(\tau_k)s_k(n) + \sum_{l=1}^{L-1} \tilde{\boldsymbol{h}}_l(\tau_k)s_k(n-l), \qquad k = 0, \ldots, K-1. \tag{20}$$

Similarly, each wideband signal will have its own upper and lower frequencies, f_k^u and f_k^l, such that T_{max} in the K-dimensional case, according to (6), is now defined as

$$T_{max} = \min_{k=0,\ldots,K-1} \left\{ \frac{1}{2f_k^u} \right\}. \tag{21}$$

We define the index $\acute{m}$ as follows

$$\acute{m} = \begin{cases} m, & \text{if} \quad \phi_k \leq \pi/2 \\ M-1-m, & \text{if} \quad \phi_k > \pi/2 \end{cases}, \tag{22}$$

such that the delayed version $s_k(t - \acute{m}\tau_k)$ the signal vector $\boldsymbol{s}(t)$ may be expressed as

$$s_k(t - \acute{m}\tau_k) = \sum_{l=0}^{L-1} h_l(\acute{m}\tau_k)s_k(n-l), \quad k = 0, \ldots, K-1. \tag{23}$$

The mth sensor output $y_m(n)$ in the presence of noise now becomes

$$y_m(n) = \sum_{k=0}^{K-1} s_k(t - \acute{m}\tau_k) + \sigma_w w_m(n), \tag{24}$$

$$= \sum_{k=0}^{K-1} \sum_{l=0}^{L-1} h_l(\acute{m}\tau_k)s_k(n-l) + \sigma_w w_m(n), \quad m = 0, \ldots, M-1, \tag{25}$$

where $\boldsymbol{s}_k(n)$ is defined as in (9) for the kth source, $w_m(n)$ is an *iid* Gaussian variable with zero mean and unit variance, and σ_w^2 is the noise variance in the observation. Using the definition (17) for $\tilde{\boldsymbol{H}}(\tau_k)$, and extending (25) for $m = 0, \ldots, M-1$, we can express the observation vector $\boldsymbol{y}(n)$ in matrix form as

$$\boldsymbol{y}(n) = \sum_{k=0}^{K-1} \tilde{\boldsymbol{H}}(\tau_k)\boldsymbol{s}_k(n) + \sigma_w \boldsymbol{w}(n), \tag{26}$$

where $\boldsymbol{w}(n) \in \mathcal{R}^M$ is a vector whose elements are $w_m(n)$.

We now define a signal vector for K sources at time n as

$$\boldsymbol{a}(n) \triangleq [s_0(n), s_1(n), \ldots, s_{K-1}(n)]^T. \tag{27}$$

Then, by extending (20) for $k = 0, ..., K-1$, we can rewrite (26) in the form

$$\boldsymbol{y}(n) \quad = \quad \tilde{\boldsymbol{H}}_0(\boldsymbol{\tau})\boldsymbol{a}(n) + \sum_{l=1}^{L-1} \tilde{\boldsymbol{H}}_l(\boldsymbol{\tau})\boldsymbol{a}(n-l) + \sigma_w \boldsymbol{w}(n), \tag{28}$$

where $\tilde{\boldsymbol{H}}_l(\boldsymbol{\tau}) \in \mathcal{R}^{M \times K}$ is defined as

$$\tilde{\boldsymbol{H}}_l(\boldsymbol{\tau}) = \left[\tilde{\boldsymbol{h}}_l(\tau_0), \tilde{\boldsymbol{h}}_l(\tau_1), \ldots, \tilde{\boldsymbol{h}}_l(\tau_{K-1})\right]. \tag{29}$$

The signal vectors $\boldsymbol{a}(n-l)$ for $l = 1, ..., L-1$ in (28) are estimated by the proposed algorithm in a manner to be described. In this vein, we define a vector $\boldsymbol{z}(n)$ as follows

$$\boldsymbol{z}(n) \triangleq \boldsymbol{y}(n) - \sum_{l=1}^{L-1} \tilde{\boldsymbol{H}}_l(\boldsymbol{\tau})\boldsymbol{a}(n-l), \tag{30}$$

which can be interpreted as the error between the snapshot $\boldsymbol{y}(n)$ and its approximation, based on the past, estimated values of the signals from $\boldsymbol{a}(n-1)$ to $\boldsymbol{a}(n-L+1)$ and the associated columns in the interpolation matrix $\boldsymbol{H}(\boldsymbol{\tau})$. Accordingly, we may rewrite (28) as follows

$$\boldsymbol{z}(n) \quad = \quad \tilde{\boldsymbol{H}}_0(\boldsymbol{\tau})\boldsymbol{a}(n) + \sigma_w \boldsymbol{w}(n), \tag{31}$$

which represents the desired form of the model.

There are several interesting features regarding the model in (31). It is similar to the familiar narrowband model [1], except that the data is modified and the steering matrix takes the form of an interpolation matrix. Further, the same model in (31) can accomodate either narrowband or wideband sources, without change of structure or parameters. Also, all quantities in (31), including the data, are pure real, unlike previous models [9] [10] [11] [12] which require complex quantities. This latter point leads to significant savings in hardware, since quadrature mixing to IF frequencies is no longer required, and computational requirements are reduced.

III. Development of The Marginal Posterior Distribution

Here, it is assumed 1) that the noise vectors $\boldsymbol{w}(n)$ are *iid* Gaussian, and 2) that all the parameters describing the received signal are stationary throughout the entire observation interval. Using (31), we may define a set of N snapshots as

$$\boldsymbol{Z} = [\boldsymbol{z}(1), \ldots, \boldsymbol{z}(N)]. \tag{32}$$

Then, the total likelihood function of all data can be expressed as follows

$$\ell(\boldsymbol{Z}|\boldsymbol{a}(\cdot), \boldsymbol{\tau}, \sigma_w^2, k) = \prod_{n=1}^{N} \frac{1}{(2\pi\sigma_w^2)^{M/2}} \exp\left\{\frac{-1}{2\sigma_w^2}\left(\boldsymbol{z}(n) - \tilde{\boldsymbol{H}}_0(\boldsymbol{\tau})\boldsymbol{a}(n)\right)^T \left(\boldsymbol{z}(n) - \tilde{\boldsymbol{H}}_0(\boldsymbol{\tau})\boldsymbol{a}(n)\right)\right\}, \tag{33}$$

where k represents an estimate of the true number of sources, K. The desired posterior distribution function can be expressed using Bayes' theorem in terms of the total likelihood function (33) and the prior distributions of the unknown parameters as

$$\pi\left(\boldsymbol{a}(\cdot),\boldsymbol{\tau},\sigma_w^2,k|\boldsymbol{Z}\right) \propto p\left(\boldsymbol{Z}|\boldsymbol{a}(\cdot),\boldsymbol{\tau},\sigma_w^2,k\right)p\left(\boldsymbol{a}(\cdot)|k,\boldsymbol{\tau},\delta^2\sigma_w^2\right)p(\boldsymbol{\tau}|k)p(\sigma_w^2)p(k), \tag{34}$$

where δ^2 is a hyper-parameter closely related to the signal–to–noise ratio. (The choice of this parameter is discussed further in Section IV-D.) The prior distribution for the source amplitude vector $\boldsymbol{a}$ is chosen as in [4]. For a single sample $\boldsymbol{a}(n)$, we take the prior distribution to be zero–mean Gaussian, with covariance matrix corresponding to the *maximum entropy* prior

$$p(\boldsymbol{a}|k,\boldsymbol{\tau},\delta^2\sigma_w^2) = \mathcal{N}\left(0,\delta^2\sigma_w^2\left[\tilde{\boldsymbol{H}}_0^T(\boldsymbol{\tau})\tilde{\boldsymbol{H}}_0(\boldsymbol{\tau})\right]^{-1}\right), \tag{35}$$

The joint prior in (34) of the source samples over N snapshots is then given as

$$p(\boldsymbol{a}(1)\ldots,\boldsymbol{a}(N)|k,\boldsymbol{\tau},\delta^2\sigma_w^2) = \prod_{n=1}^{N}\mathcal{N}\left(0,\delta^2\sigma_w^2\left[\tilde{\boldsymbol{H}}_0^T(\boldsymbol{\tau})\tilde{\boldsymbol{H}}_0(\boldsymbol{\tau})\right]^{-1}\right), \tag{36}$$

where, for analytical convenience, we have assumed the sources to be temporally *iid*. The prior distribution of $\boldsymbol{\tau}$ is chosen to be uniform

$$p(\boldsymbol{\tau}|k) = \mathcal{U}\left[-T_{max},T_{max}\right]^k. \tag{37}$$

The prior for the parameter σ_w^2 is chosen as the inverse-Gamma distribution [4], which is the conjugate prior corresponding to a Gaussian likelihood function. It is defined as

$$p(\sigma_w^2) = \mathcal{IG}\left(\frac{\nu_0}{2},\frac{\gamma_0}{2}\right) = \left(\sigma_w^2\right)^{-\frac{\nu_0}{2}-1}\exp\left\{\frac{-\gamma_0}{2\sigma_w^2}\right\}. \tag{38}$$

Note that this distribution is noninformative when $\gamma_0 = \nu_0 = 0$.[4] Finally, the prior distribution on k is chosen to be Poisson with parameter Ξ

$$p(k) = \frac{\Xi^k}{k!}\exp\left(-\Xi\right), \tag{39}$$

where Ξ is the expected number of sources. This choice of prior is not strictly noninformative, but it contributes to a more efficient MCMC sampling routine. As a result, we can rewrite (34)

[4]Strictly speaking, this choice for γ_0 and ν_0 results in an improper prior distribution. Regardless, the resulting posterior distribution still has a well-defined maximum, which is used for MAP estimation of the parameters of interest.

as

$$\pi\left(\boldsymbol{a},\boldsymbol{\tau},\sigma_w^2,k|\boldsymbol{Z}\right) \propto \frac{1}{(2\pi\sigma_w^2)^{MN/2}}\exp\left\{\frac{-1}{2\sigma_w^2}\sum_{n=1}^{N}\left(\boldsymbol{z}(n)-\tilde{\boldsymbol{H}}_0(\boldsymbol{\tau})\boldsymbol{a}(n)\right)^T\left(\boldsymbol{z}(n)-\tilde{\boldsymbol{H}}_0(\boldsymbol{\tau})\boldsymbol{a}(n)\right)\right\}\times$$
$$\frac{|\tilde{\boldsymbol{H}}_0^T(\boldsymbol{\tau})\tilde{\boldsymbol{H}}_0(\boldsymbol{\tau})|^{N/2}}{(2\pi\delta^2\sigma_w^2)^{Nk/2}}\exp\left\{\frac{-1}{2\delta^2\sigma_w^2}\sum_{n=1}^{N}\boldsymbol{a}^T(n)\tilde{\boldsymbol{H}}_0^T(\boldsymbol{\tau})\tilde{\boldsymbol{H}}_0(\boldsymbol{\tau})\boldsymbol{a}(n)\right\}\times$$
$$\left(\frac{1}{2T_{max}}\right)^k\times\frac{\Xi^k}{k!}\exp\left(-\Xi\right)\times\left(\sigma_w^2\right)^{-\frac{\nu_0}{2}-1}\exp\left\{\frac{-\gamma_0}{2\sigma_w^2}\right\}. \tag{40}$$

A. Simplification of the posterior distribution function

We can simplify the estimation of the parameters in the posterior distribution function (40) by considering $\boldsymbol{a}$ and σ_w to be nuisance parameters, and analytically integrating them out. The only quantities of interest at this stage are $\boldsymbol{\tau}$ and k. We recover the $\boldsymbol{a}$ later by other means. By following procedures similar to those in [4], [17], it can be shown that the desired posterior distribution function in (40) can be expressed as

$$\pi(\boldsymbol{a},\boldsymbol{\tau},\sigma_w^2,k|\boldsymbol{Z}) \propto \frac{1}{(2\pi\sigma_w^2)^{MN/2}}\exp\left\{\frac{-1}{2\sigma_w^2}\sum_{n=1}^{N}\boldsymbol{z}^T(n)\tilde{\boldsymbol{P}}_{H_0}^{\perp}(\boldsymbol{\tau})\boldsymbol{z}(n)\right\}\times$$
$$\frac{|\tilde{\boldsymbol{H}}_0^T(\boldsymbol{\tau})\tilde{\boldsymbol{H}}_0(\boldsymbol{\tau})|^{N/2}}{(2\pi\delta^2\sigma_w^2)^{Nk/2}}\exp\left\{\frac{-1}{2\sigma_w^2}\sum_{n=1}^{N}\left(\boldsymbol{a}(n)-\boldsymbol{m}_a(n)\right)^T\tilde{\boldsymbol{\Sigma}}_{H_0}^{-1}(\boldsymbol{\tau})\left(\boldsymbol{a}(n)-\boldsymbol{m}_a(n)\right)\right\}\times$$
$$\left(\frac{\Xi}{2T_{max}}\right)^k\times\frac{1}{k!}\exp\left(-\Xi\right)\times\left(\sigma_w^2\right)^{-\frac{\nu_0}{2}-1}\exp\left\{\frac{-\gamma_0}{2\sigma_w^2}\right\}. \tag{41}$$

where

$$\tilde{\boldsymbol{\Sigma}}_{H_0}^{-1}(\boldsymbol{\tau}) = (1+\delta^{-2})\tilde{\boldsymbol{H}}_0^T(\boldsymbol{\tau})\tilde{\boldsymbol{H}}_0(\boldsymbol{\tau}), \tag{42}$$

$$\tilde{\boldsymbol{P}}_{H_0}^{\perp}(\boldsymbol{\tau}) = \boldsymbol{I} - \frac{\tilde{\boldsymbol{H}}_0(\boldsymbol{\tau})\left[\tilde{\boldsymbol{H}}_0^T(\boldsymbol{\tau})\tilde{\boldsymbol{H}}_0(\boldsymbol{\tau})\right]^{-1}\tilde{\boldsymbol{H}}_0^T(\boldsymbol{\tau})}{(1+\delta^{-2})}, \tag{43}$$

and

$$\begin{aligned}\boldsymbol{m}_a(n) &= \tilde{\boldsymbol{\Sigma}}_{H_0}(\boldsymbol{\tau})\tilde{\boldsymbol{H}}_0^T(\boldsymbol{\tau})\boldsymbol{z}(n),\\ &= \tilde{\boldsymbol{\Sigma}}_{H_0}(\boldsymbol{\tau})\tilde{\boldsymbol{H}}_0^T(\boldsymbol{\tau})\left(\boldsymbol{y}(n)-\sum_{l=1}^{L-1}\tilde{\boldsymbol{H}}_l(\boldsymbol{\tau})\boldsymbol{a}(n-l)\right).\end{aligned} \tag{44}$$

From (44) and (41) a *maximum a posteriori* estimate of the amplitudes, given the other parameters is readily available as

$$\hat{\boldsymbol{a}}_{MAP}(n) \triangleq \boldsymbol{m}_a(n). \tag{45}$$

We can simplify (41) by analytically integrating out the nuisance parameters $\boldsymbol{a}(n)$ and σ_w^2 as follows

$$\pi(\boldsymbol{\tau}, k|\boldsymbol{Z}) \quad \propto \quad \int_0^\infty \int_{-\infty}^\infty p(\boldsymbol{a}, \boldsymbol{\tau}, \sigma_w^2, k|\boldsymbol{Z}) d\boldsymbol{a} d\sigma_w^2. \tag{46}$$

As a result, the desired posterior distribution can now be expressed as [4]

$$\pi(\boldsymbol{\tau}, k|\boldsymbol{Z}) \quad \propto \quad \frac{1}{(1+\delta^2)^{Nk/2}} \left(\frac{\Xi}{2T_{max}}\right)^k \frac{\exp(-\Xi)}{k!} \left(\gamma_0 + \mathrm{tr}\left(\tilde{\boldsymbol{P}}_{\mathrm{H}_0}^{\perp}(\boldsymbol{\tau}) \hat{\boldsymbol{R}}_{\mathrm{zz}}\right)\right)^{-\left(\frac{MN+\nu_0}{2}\right)}, \tag{47}$$

where $\mathrm{tr}(\cdot)$ is the trace operator, and

$$\mathrm{tr}\left(\tilde{\boldsymbol{P}}_{\mathrm{H}_0}^{\perp}(\boldsymbol{\tau}) \hat{\boldsymbol{R}}_{\mathrm{zz}}\right) = \sum_{n=1}^{N} \boldsymbol{z}^T(n) \tilde{\boldsymbol{P}}_{H_0}^{\perp}(\boldsymbol{\tau}) \boldsymbol{z}(n), \tag{48}$$

and $\hat{\boldsymbol{R}}_{zz}$ is the sample covariance matrix of $\boldsymbol{z}(n)$

$$\hat{\boldsymbol{R}}_{zz} = \sum_{n=1}^{N} \boldsymbol{z}(n) \boldsymbol{z}^T(n). \tag{49}$$

The primary goal of this work is to estimate the delay parameters $\boldsymbol{\tau}$ and the model order k using the distribution of (47). Because there are no direct methods for estimating model order for this problem, and because of the intractable form of this distribution, MCMC methods [4], [17], [19] , as described in the next section, are well-suited for this task.

The proposed MCMC methods require evaluation of the posterior distribution (47) for a proposed value of $\boldsymbol{\tau}$ and k. This involves evaluation of the quantity $\hat{\boldsymbol{R}}_{zz}$, which in turn requires knowledge of the source amplitudes $\boldsymbol{a}(n)$. The amplitudes can in principle be determined through a least–squares procedure using (31), or through (45). However, the use of (31) involves only the matrix $\tilde{\boldsymbol{H}}_0(\boldsymbol{\tau})$ (instead of all the matrices $\tilde{\boldsymbol{H}}_0(\boldsymbol{\tau}), \ldots, \tilde{\boldsymbol{H}_{L-1}}(\boldsymbol{\tau})$). For typical interpolation functions, only a few elements of each of the columns of $\tilde{\boldsymbol{H}}_0(\boldsymbol{\tau})$ will be significantly different from zero, resulting in a portion of the observation vector being suppressed, with a corresponding loss of performance. Further, use of (45) also implicitly involves only the matrix $\tilde{\boldsymbol{H}}_0(\boldsymbol{\tau})$. This is because the term within parentheses in (44) is equal to $\tilde{\boldsymbol{H}}_0(\boldsymbol{\tau})\boldsymbol{a}(n) + \sigma_w w(n)$. All other terms in (45) only involve $\tilde{\boldsymbol{H}}_0(\boldsymbol{\tau})$. Thus, use of (45) also results in a degradation in performance. This undesired situation can be mitigated using the following suboptimal procedure for estimating the source amplitudes.

B. Signal Recovery

According to the signal model, it is clear that the source sample $\boldsymbol{a}(n-L+1)$ contributes to L successive snapshots $\boldsymbol{y}(n-L+1)$ to $\boldsymbol{y}(n)$. Efficient estimation of the source sample $\boldsymbol{a}(n-L+1)$ requires use of all these snapshots. From (28), we have

$$\boldsymbol{y}(n) = \sum_{l=0}^{L-1} \tilde{\boldsymbol{H}}_l(\boldsymbol{\tau}) \boldsymbol{a}(n-l) + \sigma_w \boldsymbol{w}(n), \tag{50}$$

The natural log of the posterior in (40) can therefore be written as

$$L(\boldsymbol{a},\boldsymbol{\tau},\sigma_w^2,k|\boldsymbol{Z}) \propto \kappa - \frac{1}{2\sigma_w^2}\sum_{n=1}^{N}\left(\boldsymbol{y}(n)-\sum_{l=0}^{L-1}\tilde{\boldsymbol{H}}_l(\boldsymbol{\tau})\boldsymbol{a}(n-l)\right)^T\left(\boldsymbol{y}(n)-\sum_{l=0}^{L-1}\tilde{\boldsymbol{H}}_l(\boldsymbol{\tau})\boldsymbol{a}(n-l)\right) - \frac{\delta^{-2}}{2\sigma_w^2}\sum_{n=1}^{N}\boldsymbol{a}^T(n)\tilde{\boldsymbol{H}}_l^T(\boldsymbol{\tau})\tilde{\boldsymbol{H}}_l(\tau)\boldsymbol{a}(n), \tag{51}$$

where κ is a constant independent of $\boldsymbol{a}(n)$. The desired estimate $\hat{\boldsymbol{a}}(n-L+1)$ is then obtained by maximizing (51) with respect to $\boldsymbol{a}(n-L+1)$. The result is

$$\hat{\boldsymbol{a}}(n-L+1) = (1+\delta^{-2})^{-1}\left[\tilde{\boldsymbol{\mathcal{H}}}^T(\boldsymbol{\tau})\tilde{\boldsymbol{\mathcal{H}}}(\boldsymbol{\tau})\right]^{-1}\tilde{\boldsymbol{\mathcal{H}}}^T(\boldsymbol{\tau})\boldsymbol{\epsilon}(n), \tag{52}$$

where

$$\tilde{\boldsymbol{\mathcal{H}}}(\boldsymbol{\tau}) = \left[\tilde{\boldsymbol{H}}_{L-1}^T(\boldsymbol{\tau}),\ldots,\tilde{\boldsymbol{H}}_1^T(\boldsymbol{\tau}),\tilde{\boldsymbol{H}}_0^T(\boldsymbol{\tau})\right]^T. \tag{53}$$

and

$$\boldsymbol{\epsilon}(n) = \left[\boldsymbol{\epsilon}_0(n),\boldsymbol{\epsilon}_1(n),\ldots,\boldsymbol{\epsilon}_{L-1}(n)\right]^T. \tag{54}$$

The quantity $\boldsymbol{\epsilon}_p(n), p=0,\ldots,L-1$ removes the contribution from samples other than $\boldsymbol{a}(n-L+1)$ in the observation $\boldsymbol{y}(n-p)$. It is defined as

$$\begin{aligned}\boldsymbol{\epsilon}_p(n) &= \boldsymbol{y}(n-p)-\boldsymbol{x}_p(n),\\ &= \tilde{\boldsymbol{H}}_{L-1-p}(\boldsymbol{\tau})\boldsymbol{a}(n-L+1)+\sigma_w\boldsymbol{w}(n),\end{aligned} \tag{55}$$

where

$$\boldsymbol{x}_p(n) \triangleq \sum_{l\neq p}^{L-1}\tilde{\boldsymbol{H}}_l(\boldsymbol{\tau})\boldsymbol{a}(n-p-l). \tag{56}$$

The $\boldsymbol{\epsilon}_p(n)$ are determined by evaluating the $\boldsymbol{x_p}(n)$ in (56), where the unknown quantities $\boldsymbol{a}(n-p-l)$ for $n-p-l > n-L+1$ in (56) are tentatively estimated suboptimally using (44) and (45). The estimation of $\boldsymbol{a}$ according to (52) results in significantly improved performance compared to the other, more direct methods for the estimation of this parameter.

The MCMC procedure described in the next section proposes a candidate sample $(\boldsymbol{\tau}^\star, k^\star)$ and requires evaluation of the posterior distribution given by (47) for that candidate. The following schema summarizes the process used for this evaluation.

Evaluation of the Posterior Density

1. Given a candidate sample ($\boldsymbol{\tau}^\star$, $k^\star$) from the MCMC procedure, and a suitable interpolation function such as a windowed $sinc(\cdot)$, compute $\tilde{\boldsymbol{H}}_l(\boldsymbol{\tau}^\star), l=0,\ldots,L-1$ of order $k^\star$ from (29).
2. For sample index $n = L-1,\ldots,N$

- Follow the steps described in Section III-B to obtain $\hat{\boldsymbol{a}}(n-L+1)$, in (52).
- Given the source amplitudes, evaluate $\boldsymbol{z}(n-L+1)$ according to (30).

3. Given the $\boldsymbol{z}(n)$, $\boldsymbol{R}_{zz}$ in (49) can be computed, which allows evaluation of the posterior density $\pi(\boldsymbol{\tau}, k|\boldsymbol{Z})$ in (47). This quantity is then used by the MCMC procedure to determine whether the candidate ($\boldsymbol{\tau}^\star$, $k^\star$) is accepted as a sample.

■

The computational requirements of the above algorithm are mitigated by the fact that the matrix $(1+\delta^{-2})^{-1}\left[\tilde{\boldsymbol{\mathcal{H}}}^T(\boldsymbol{\tau})\tilde{\boldsymbol{\mathcal{H}}}(\boldsymbol{\tau})\right]^{-1}\tilde{\boldsymbol{\mathcal{H}}}^T(\boldsymbol{\tau})$ in (52) is independent of n and therefore need only be computed once per MCMC iteration.

IV. Reversible Jump MCMC

MCMC methods [19], [17] are numerical techniques for performing Bayesian estimation, inference, or detection, corresponding to an arbitrary distribution of interest. In the Bayesian framework, one is commonly faced with the integration of unwanted model parameters, or with task of evaluating expectations for the purpose of parameter estimation. In the general case, the posterior distribution of interest exhibits some degree of nonlinearity and involves a large number of parameters, making the analytical closed-form evaluation of these integrations difficult. One of the major advantages of MCMC methods is that these integrations become trivial to perform. The basic idea behind MCMC methods is to draw samples from a posterior distribution of interest, in effect forming a histogram, and then form sample averages to approximate expectations, thus facilitating parameter estimation [19]. Also, once the histogram is available, marginalization of unwanted parameters is straightforward. The samples are generated by setting up a Markov chain, whose invariant distribution is the posterior distribution $\pi(\boldsymbol{x})$ of interest. Thus, each state of the chain corresponds to a potential sample from $\pi(\boldsymbol{x})$.

The critical component of an MCMC method is an algorithm to draw samples from an arbitrary distribution. Here, we choose the Metropolis-Hastings (M-H) algorithm [22], [19] for this purpose. At each iteration step i of the Markov chain, the next state $\boldsymbol{\tau}^{(i+1)}$ is chosen by first sampling a *candidate* state $\boldsymbol{\tau}^\star$ from a *proposal* distribution $q(\cdot|\boldsymbol{\tau})$. The proposal distribution may depend on the current state of the Markov chain $\boldsymbol{\tau}$. The candidate state $\boldsymbol{\tau}^\star$ is then *accepted* with probability

$$\alpha(\boldsymbol{\tau}, \boldsymbol{\tau}^\star) = \min\left\{1, r(\boldsymbol{\tau}, \boldsymbol{\tau}^\star)\right\}, \tag{57}$$

where $r(\boldsymbol{\tau}, \boldsymbol{\tau}^\star)$ is the *acceptance ratio*, defined as

$$r(\boldsymbol{\tau}, \boldsymbol{\tau}^\star) = \frac{\pi(\boldsymbol{\tau}^\star)q(\boldsymbol{\tau}|\boldsymbol{\tau}^\star)}{\pi(\boldsymbol{\tau})q(\boldsymbol{\tau}^\star|\boldsymbol{\tau})}. \tag{58}$$

The proposal function $q(\cdot)$ is chosen to be easy to sample from, and must be non-null over the support of the distribution $\pi(\cdot)$. If the candidate is accepted, the next state of the chain will be $\boldsymbol{\tau}^{(i+1)} = \boldsymbol{\tau}^\star$. If the candidate is rejected, the chain remains in state $\boldsymbol{\tau}^{(i+1)} = \boldsymbol{\tau}^{(i)}$.

A Markov chain generally exhibits a transient period before its states converge to the invariant distribution of the chain. In practice, this means the initial samples produced by the MCMC procedure (referred to as the *burn-in* period [19]) must be discarded.

We use the *reversible jump* MCMC algorithm [20], [17] to perform the Bayesian computation in jointly detecting the desired model order and extracting the other parameters of interest from the posterior distribution. The reversibile jump MCMC algorithm itself is similar to the M-H algorithm, but it allows the sampling process to jump between subspaces of different dimensions, which facilitates the detection of model order. Denote the whole parameter space by $\cup_{k=0}^{k_{max}} k \times \boldsymbol{\Phi}_k$, where $\boldsymbol{\Phi}_k$ is the space of the parameters of the model of order k, and k_{max} is the maximum allowable model order. At each iteration, candidate samples are chosen from a set of proposal distributions corresponding to different model orders, which are randomly accepted according to an acceptance ratio similar to that of (58), given by

$$r((\boldsymbol{\tau}^\star, k^\star), (\boldsymbol{\tau}, k)) = \frac{\pi(\boldsymbol{\tau}^\star, k^\star) q(\boldsymbol{\tau}, k | \boldsymbol{\tau}^\star, k^\star)}{\pi(\boldsymbol{\tau}, k) q(\boldsymbol{\tau}^\star, k^\star | \boldsymbol{\tau}, k)} \times \boldsymbol{J}((\boldsymbol{\tau}^\star, k^\star), (\boldsymbol{\tau}, k)), \tag{59}$$

where it can be shown [23] that in our case, $\boldsymbol{J}((\boldsymbol{\tau}^\star, k^\star), (\boldsymbol{\tau}, k)) = 1$. This quantity is the Jacobian of the transformation, required to reconcile the total probability between spaces of different dimensions so that the reversibility condition is satisfied. If the candidate is accepted, the chain takes the new state; otherwise the chain remains at the current state.

In the reversible jump algorithm, we choose our set of proposal distributions to correspond to the following set of moves

1. the *birth* move, valid for $k < M$. Here, a new τ is proposed at random on $[-T_{max}, T_{max}]$.
2. the *death* move, valid for $k > 0$. Here, a τ is randomly chosen to be removed.
3. the *update* move. Here, the order of the model is held fixed and the parameters describing the sources are updated.

The probabilities for choosing each move are denoted by u_k, b_k, and d_k, respectively, such that $u_k + b_k + d_k = 1$ for all k. In accordance with [4], we choose

$$b_k = c \min\left\{\frac{p(k+1)}{p(k)}, 1\right\}, \quad d_{k+1} = c \min\left\{\frac{p(k)}{p(k+1)}, 1\right\}, \tag{60}$$

where $p(\cdot)$ is the prior distribution of the kth model according to (39), and c is a tuning parameter which determines the ratio of update moves to jump moves. We choose $c = 0.5$ so that the probability of a jump is between 0.5 and 1 at each iteration [20] . The overall description of the reversible jump MCMC algorithm is determined by the choice of move at each iteration. This description is summarized as follows

---

Reversible Jump MCMC

1. Initialization: set $\boldsymbol{\Phi}^{(i=0)} = \left(\boldsymbol{\tau}^{(i=0)}, k^{(i=0)}\right)$, where i is the iteration index
2. Iteration i

- Sample $u \sim U_{[0,1]}$,
- Compute $b_{k^{(i)}}$ and $d_{k^{(i)}}$ according to (60), using the value of $k^{(i)}$, which is the model order of the ith iteration.
- if $(u < b_{k^{(i)}})$ then execute a "birth move" (see Section IV-B),
- else if $(u < b_{k^{(i)}} + d_{k^{(i)}})$ then execute a "death move" (see Section IV-C),
- else, execute an update move (see Section IV-A).

3. $i \leftarrow i + 1$, goto step 2

We now give details for each move type.

A. Update Move

Here, we assume that the current state of the algorithm is in $\{\boldsymbol{\Phi}_k, k\}$. When the update move is selected, the algorithm samples only on the space of $\boldsymbol{\Phi}_k$ for a fixed k. The acceptance function for an update move is defined using (58) as

$$r_{update} = \frac{\pi(\boldsymbol{\tau}_k^\star|\boldsymbol{Z}^\star)q(\boldsymbol{\tau}_k|\boldsymbol{\tau}_k^\star)}{\pi(\boldsymbol{\tau}_k|\boldsymbol{Z})q(\boldsymbol{\tau}_k^\star|\boldsymbol{\tau}_k)}, \tag{61}$$

where

$$q(\boldsymbol{\tau}_k|\boldsymbol{\tau}_k^\star) = p(\boldsymbol{\tau}|k) = p(\boldsymbol{\tau}^\star|k), \tag{62}$$

and $p(\tau|k)$ is the prior density for τ given by (37). Accordingly, substituting (47) into (61) yields

$$r_{update} = \frac{\pi(\boldsymbol{\tau}_k^\star|\boldsymbol{Z}^\star)}{\pi(\boldsymbol{\tau}_k|\boldsymbol{Z})}, \tag{63}$$

$$= \left(\frac{\gamma_0 + \mathrm{tr}\left(\tilde{\boldsymbol{P}}_{H_0}^{\perp}(\boldsymbol{\tau}_k)\hat{\boldsymbol{R}}_{zz}\right)}{\gamma_0 + \mathrm{tr}\left(\tilde{\boldsymbol{P}}_{H_0}^{\perp}(\boldsymbol{\tau}_k^\star)\hat{\boldsymbol{R}}_{zz}^\star\right)}\right)^{\frac{MN+\nu_0}{2}}. \tag{64}$$

The candidate $\boldsymbol{\tau}_k^\star$ is then accepted as the current state $\boldsymbol{\tau}_k^{(i+1)} = \boldsymbol{\tau}_k^\star$, with probability

$$\alpha_{update}\left(\boldsymbol{\tau}_k, \boldsymbol{\tau}_k^\star\right) = \min\left\{1, r_{update}\right\}. \tag{65}$$

In each iteration, a candidate $\boldsymbol{\tau}_k^\star$ is first sampled according to (62). Then, the schema in Sect. IIIB is executed which then allows evaluation of r_{update} and α_{update}.

B. Birth Move

In the birth move, we assume the state of the algorithm is in $\{\boldsymbol{\Phi}_k, k\}$ at the present ith iteration, and we wish to determine whether the state is in $\{\boldsymbol{\Phi}_{k+1}, k+1\}$ at the next iteration. The acceptance ratio of the birth move is therefore defined as

$$r_{birth} = \frac{\pi(\boldsymbol{\tau}_{k+1}^\star, k+1|\boldsymbol{Z})q(\boldsymbol{\tau}_k, k|\boldsymbol{\tau}_{k+1}^\star, k+1)}{\pi(\boldsymbol{\tau}_k, k|\boldsymbol{Z})q(\boldsymbol{\tau}_{k+1}^\star, k+1|\boldsymbol{\tau}_k, k)}. \tag{66}$$

We propose a delay vector $\boldsymbol{\tau}^\star$ as

$$\boldsymbol{\tau}^\star_{k+1} = \left[\boldsymbol{\tau}^{(i)}_k, \tau_c\right], \tag{67}$$

where $\boldsymbol{\tau}^{(i)}_k$ is the delay vector at the ith iteration, and τ_c is a new time delay candidate selected uniformly on $[-T_{max}, T_{max}]$. Note that the prior for model order k in (39) is assumed independent of that for $\boldsymbol{\tau}$ in (37). In the birth move, only the one new source is a random variable; the remaining sources are treated as constants. Accordingly, the proposal distribution $q\left(\boldsymbol{\tau}^\star_{k+1}, k+1|\boldsymbol{\tau}_k, k\right)$ from (66) is then

$$q\left(\boldsymbol{\tau}^\star_{k+1}, k+1|\boldsymbol{\tau}_k, k\right) = p(k+1) \times \frac{1}{2T_{max}}. \tag{68}$$

In contrast, the the distribution $q(k, \boldsymbol{\tau}_k|k+1, \boldsymbol{\tau}^\star_{k+1})$ in (66) refers to the proposal distribution where one of the $k+1$ sources is randomly removed. Note that in this case, there is no randomness in $\boldsymbol{\tau}$. Thus, we have

$$q(\boldsymbol{\tau}_k, k|\boldsymbol{\tau}^\star_{k+1}, k+1) = p(k) \times \frac{1}{k+1}. \tag{69}$$

As a result, the ratio of proposal functions in (66) becomes

$$\frac{q(\boldsymbol{\tau}_k, k|\boldsymbol{\tau}^\star_{k+1}, k+1)}{q(\boldsymbol{\tau}^\star_{k+1}, k+1|\boldsymbol{\tau}_k, k)} = \frac{2T_{max}}{\Xi}, \tag{70}$$

and the acceptance ratio r_{birth} becomes

$$\begin{aligned} r_{birth} &= \frac{\pi(\boldsymbol{\tau}^\star_{k+1}, k+1|\boldsymbol{Z}^\star)}{\pi(\boldsymbol{\tau}_k, k|\boldsymbol{Z})} \times \frac{2T_{max}}{\Xi}, \\ &= \left(\frac{\gamma_0 + \mathrm{tr}\left(\tilde{\boldsymbol{P}}^\perp_{H_0}(\boldsymbol{\tau}_k)\hat{\boldsymbol{R}}_{zz}\right)}{\gamma_0 + \mathrm{tr}\left(\tilde{\boldsymbol{P}}^\perp_{H_0}(\boldsymbol{\tau}^\star_{k+1})\hat{\boldsymbol{R}}^\star_{zz}\right)}\right)^{\frac{MN+\nu_0}{2}} \times \frac{1}{(1+\delta^2)^{N/2}} \times \frac{1}{k+1}. \end{aligned} \tag{71}$$

The probability of accepting a birth move is therefore defined as

$$\alpha_{birth} = \min\left\{1, r_{birth}\right\}. \tag{72}$$

As in the update move, in each iteration a candidate $\boldsymbol{\tau}^\star_{k^\star}$ for $k^\star = k+1$ is first sampled according to (62). The acceptance ratio is evaluated by executing the schema of Sect. III-B, and then evaluating (71).

C. Death Move

In the death move, we assume the state of the algorithm is in $\{\boldsymbol{\Phi}_{k+1}, k+1\}$ at the ith iteration, and we wish to determine whether the state is in $\{\boldsymbol{\Phi}_k, k\}$ at the next iteration.

In order to maintain the invariant distribution of the reversible jump MCMC algorithm with respect to model order, the Markov chain must be *reversible* with respect to moves across subspaces of different model orders. That is, the probability of moving from model order k to

$k+1$ must be equal to that of moving from $k+1$ to k. Therefore we propose a death move in which a source in the current state $(\boldsymbol{\tau}_{k+1}, k+1)$ is randomly selected to be removed such that the state becomes $(\boldsymbol{\tau}_k, k)$ at the next iteration. In the death move, the roles of the candidate $(\boldsymbol{\tau}^\star, k^\star)$ and the current state of the chain $(\boldsymbol{\tau}, k)$ are reversed with respect to the birth move in the corresponding expression for the acceptance ratio. Therefore, with respect to (66), the acceptance ratio for the death move is defined as

$$r_{death} = \frac{1}{r_{birth}}, \tag{73}$$

which is a sufficient condition for reversibility with respect to model order [20], and the new candidate of dimension k is accepted with probability

$$\alpha_{death} = \min\left\{1, r_{death}\right\}. \tag{74}$$

D. Model Order Determination

Even though δ^2 in (34) is an estimate of the SNR, in practice it is generally an unknown quantity. Therefore, in this section we discuss conditions which must be placed on this hyper-parameter to achieve consistent determination of the model order. According to the simplified posterior distribution in (47), we can obtain the marginal posterior distribution for model order k as:

$$\pi(k|\boldsymbol{Z}) \quad \propto \quad \int \pi(\boldsymbol{\tau}, k|\boldsymbol{Z}) d\boldsymbol{\tau}. \tag{75}$$

Denoting the true model order and delay values by k_0 and $\boldsymbol{\tau_0}$ respectively, we perform the following eigendecomposition, at $\boldsymbol{\tau} = \boldsymbol{\tau_0}$:

$$\tilde{\boldsymbol{P}}^{\perp}_{H_0}(\boldsymbol{\tau_0}) \hat{\boldsymbol{R}}_{zz} \tilde{\boldsymbol{P}}^{\perp^T}_{H_0}(\boldsymbol{\tau_0}) = \boldsymbol{Q}(\boldsymbol{\tau_0}) \Lambda(\boldsymbol{\tau_0}) \boldsymbol{Q}^T(\boldsymbol{\tau_0}), \tag{76}$$

where $\boldsymbol{Q}(\boldsymbol{\tau_0})$ is an orthonormal matrix which contains the $M-k$ eigenvectors associated with the $M-k$ smallest (noise) eigenvalues of the matrix $\hat{\boldsymbol{R}}_{zz}$, which are placed in the diagonal matrix, $\boldsymbol{\Lambda}(\boldsymbol{\tau_0})$:

$$\boldsymbol{\Lambda}(\boldsymbol{\tau_0}) = \mathrm{diag}\left[\lambda_1, \lambda_2, \ldots, \lambda_{\mathrm{M-k}}\right]. \tag{77}$$

For convenience, these eigenvalues λ_i, $i = 1, 2, ..., M-k$ are arranged in *assending* order. Assuming that N is large, and that the SNR level is moderate, then the posterior distribution function $\pi(\boldsymbol{\tau}, k|\boldsymbol{Z})$ concentrates around the true value $\boldsymbol{\tau_0}$. As a result, we can approximate the integral in (75) in the neighbourhood of $\boldsymbol{\tau_0}$ as follows

$$\pi(k|\boldsymbol{Z}) \quad \dot{\propto} \quad \frac{1}{(1+\delta^2)^{Nk/2}} \left(\frac{\Xi}{2T_{max}}\right)^k \frac{\exp\left(-\Xi\right)}{k!} \left(\gamma_0 + \sum_{i=1}^{M-k} \lambda_i\right)^{-\left(\frac{MN+\nu_0}{2}\right)}, \tag{78}$$

where $\dot{\propto}$ indicates "approximately proportional to."

Let us define the event E_i as the declaration of a model order in error by i signals. Thus, the event E_i will occur if we declare $\hat{k} = k_0 + i$ or $\hat{k} = k_0 - i$. We assume $P(E_1) > P(E_2) > \cdots > P(E_{M-1})$. Accordingly, sufficient conditions which must be satisfied for consistent detection of the model order are:

$$\lim_{N\to\infty} \frac{\pi(k_0+1|\boldsymbol{Z})}{\pi(k_0|\boldsymbol{Z})} \;\; \rightarrow \;\; 0, \tag{79}$$

$$\lim_{N\to\infty} \frac{\pi(k_0-1|\boldsymbol{Z})}{\pi(k_0|\boldsymbol{Z})} \;\; \rightarrow \;\; 0. \tag{80}$$

From (47), we have

$$\frac{\pi(k_0+1|\boldsymbol{Z})}{\pi(k_0|\boldsymbol{Z})} \;\; = \;\; \frac{\Xi}{2T_{max}} \times \frac{1}{(k_0+1)(1+\delta^2)^{N/2}} \left(\frac{\gamma_0 + \sum_{i=1}^{M-k_0-1} \lambda_i}{\gamma_0 + \sum_{i=1}^{M-k_0} \lambda_i} \right)^{-\left(\frac{MN+\nu_0}{2}\right)}, \tag{81}$$

and

$$\frac{\pi(k_0-1|\boldsymbol{Z})}{\pi(k_0|\boldsymbol{Z})} \;\; = \;\; \frac{2T_{max}}{\Xi} \times k_0(1+\delta^2)^{N/2} \left(\frac{\gamma_0 + \sum_{i=1}^{M-k_0+1} \lambda_i}{\gamma_0 + \sum_{i=1}^{M-k_0} \lambda_i} \right)^{-\left(\frac{MN+\nu_0}{2}\right)}. \tag{82}$$

From (81), we can see that (79) is satisfied if

$$1+\delta^2 > \left(\frac{\gamma_0 + \sum_{i=1}^{M-k_0} \lambda_i}{\gamma_0 + \sum_{i=1}^{M-k_0-1} \lambda_i} \right)^{M}. \tag{83}$$

Similarly, from (82) we can see that (80) is satisfied if

$$1+\delta^2 < \left(\frac{\gamma_0 + \sum_{i=1}^{M-k_0+1} \lambda_i}{\gamma_0 + \sum_{i=1}^{M-k_0} \lambda_i} \right)^{M}. \tag{84}$$

Note that the argument on the right in (83) that only contains noise eigenvalues is very close to one, whereas that in (84) contains the smallest signal eigenvalue and the noise eigenvalues is significantly larger than one. Therefore, from (83) and (84) we have

$$\left(\frac{\gamma_0 + \sum_{i=1}^{M-k_0} \lambda_i}{\gamma_0 + \sum_{i=1}^{M-k_0-1} \lambda_i} \right)^{M} < 1+\delta^2 < \left(\frac{\gamma_0 + \sum_{i=1}^{M-k_0+1} \lambda_i}{\gamma_0 + \sum_{i=1}^{M-k_0} \lambda_i} \right)^{M}. \tag{85}$$

Therefore, the specific range of the hyper-parameter δ^2 is dependent on the number of sensors, M, and the current SNR level. Note that as δ^2 is set too small, the expression in (81) will not converge to zero. Thus, it is possible for the algorithm to overestimate the model order as $\pi(k_0+1|\boldsymbol{Z})$ is comparable to $\pi(k_0|\boldsymbol{Z})$. Likewise, if δ^2 is set too large, the expression in (82) will not converge to zero. As a result, the algorithm can underestimate the model order when $\pi(k_0-1|\boldsymbol{Z})$ is comparable to $\pi(k_0|\boldsymbol{Z})$.

Referring to (85), the determination of the correct value of δ^2 requires the knowledge of the true model order k_0. However, we can still obtain useful information from (85) by having an

Parameter	SNR (dB)	M	K	L	N	σ_w^2	δ^2	F_s (Hz)	$\boldsymbol{\theta}$ (deg)	$\boldsymbol{\tau}$ (sec)
Value	14	8	2	8	50	0.0169	50	1,000	$[-3.44, 3.44]$	$[-7.5, 7.5] \times 10^{-5}$

TABLE 5.1

Parameters for the experiments.

estimate of the SNR level. This is a reasonable assumption, as we can obtain an estimate of the noise level by listening for the power level when it is assumed there is no signal present. Similarly, we can get an estimate of signal power by listening when the signal is transmitting. Thus, the right limit in (85) can be approximated if there is some knowledge of the SNR level. In practice, the left–hand term in (85) is close to unity. With this knowledge, we can obtain a reasonable estimate of the range within which δ^2 must fall.

V. Simulation Results

The proposed algorithm is now applied to two scenarios. One is wideband and the other narrowband. In each scenerio, snapshots are generated using (26) with the parameters described in Tables 5.1 to jointly detect and estimate the relevant parameters $(\boldsymbol{\tau}, k)$ and the source amplitudes $\boldsymbol{s}_k(n)$. In these experiments, the model order k and the delay parameters $\boldsymbol{\tau}$ are kept constant throughout the entire observation period. To set up the corresponding interpolation matrix for a set of $\boldsymbol{\tau}$, a *sinc* function is chosen such that the (m, l)th element of the interpolation matrix for the kth source is given by

$$\left[\tilde{\boldsymbol{H}}\right]_{m,l}(\tau_k) = \frac{\sin\left(\pi f_c\left(lT_s - m\tau_k\right)\right)}{\pi f_c\left(lT_s - m\tau_k\right)} \times W\left(lT_s - m\tau_k\right), \tag{86}$$

where T_s is the sampling interval, f_c is the cutoff frequency and $W(\cdot)$ is a Hamming window function. In all experiments, the hyper-parameters γ_0 and ν_0 are set to zero.

A. Experiment 1: Wideband Scenario

In this experiment, we generate $K = 2$ Gaussian processes for the sources that are zero mean with variance $\delta^2\sigma_w^2$, and bandlimited as follows

$$f \in [100, 400]\,\text{Hz}, \tag{87}$$

where the bandwidth of the signals is 300 Hz. According to (5), the interspacing of two adjacent sensors, Δ, can be determined as

$$\Delta = \frac{1}{2}\lambda_{min} = \frac{C}{800}. \tag{88}$$

The incident angles are -3.44 and 3.44 degrees, respectively, which are separated by an angle less than a standard half-beamwidth. A standard beamwidth is given as [1]

$$\Delta BW = \sin^{-1}\left(\frac{\lambda}{M\Delta}\right) = \sin^{-1}\left(\frac{1}{4}\right) = 14.18^\circ, \tag{89}$$

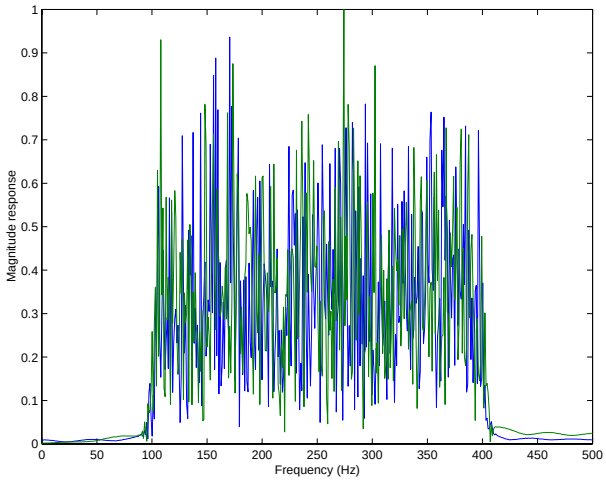

Fig. 3. The magnitude responses of the wideband signals that are bandlimited within 100 and 400 Hz.

where $\Delta = \lambda/2$. Using the definition in (3), we can obtain the corresponding ISD parameters as follows

$$\boldsymbol{\tau} = \frac{\Delta}{C} \sin \boldsymbol{\theta} = [-7.5, 7.5] \times 10^{-5}. \tag{90}$$

We can then generate $N = 50$ snapshots, according to the other parameters in Table 5.1. Fig. 3 exhibits the magnitude spectrum of the generated wideband signals. The hyper-parameter δ^2 is assumed known and is chosen as follows

$$\delta^2 = 50, \tag{91}$$

which is within the bounds specified by (85). The proposal distribution $q(\tau, k)$ used for these experiments is given by

$$q(\tau, k) = p(k) \cdot p(\tau|k) \tag{92}$$

where $p(\tau|k)$ and $p(k)$ are the prior distributions given respectively by (37) and (39).

The proposed algorithm randomly initializes all unknown parameters, and randomly assigns the initial model order k uniformly in $[1, k_{max}]$, where $k_{max} = M - 1 = 7$, is the maximum allowable model order. The number of MCMC iterations used in the algorithm is 10,000. Fig. 4 exhibits the resulting histogram for the number of sources, from which the algorithm predicts the correct number of sources, $k = 2$, whereas Fig. 5 displays the estimate of the number of sources for each iteration as the algorithm proceeds. The algorithm takes about 25 iterations to converge to the correct order. However, the algorithm takes about 2,000 iterations for a burn-in before the chain centres on the true ISD values. Note that the burn-in period is determined empirically.

Fig. 6 depicts a comparison between the ISD estimates of the sources and the true values after the burn-in stage, versus iteration number. It is clear that the chain centers on the true ISD values. Fig. 7 shows the marginal histograms of the ISDs from which the MAP estimates

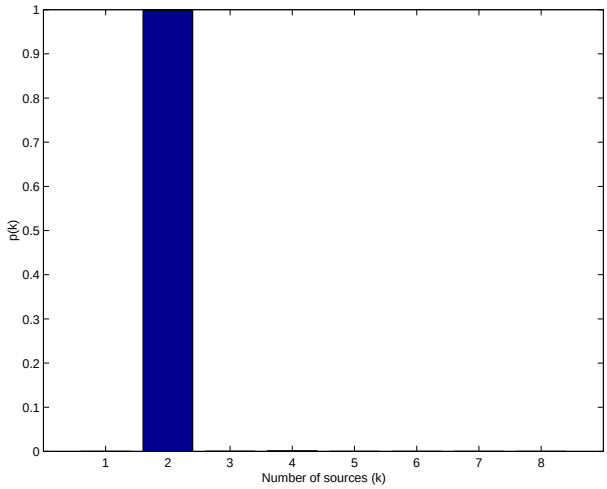

Fig. 4. Histogram of the number of sources after burn-in.

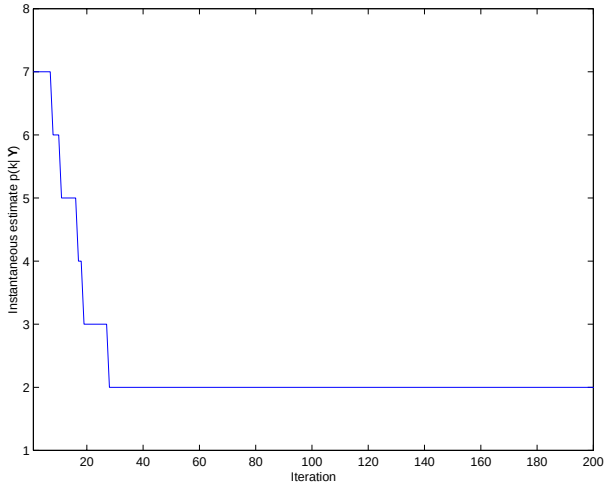

Fig. 5. Instantaneous estimate of $p(k|\boldsymbol{Y})$, for the first 200 iterations of the chain.

are obtained. As a result, the MAP delay estimates $\boldsymbol{\tau}$ from the above simulation are shown in Table 5.2, which also summarizes a comparison between the true and estimated values of the incident angles and the corresponding ISD parameters. Given the MAP estimate of the ISDs $\boldsymbol{\tau}$, the algorithm can now restore the source signals, as shown in Fig. 8. It is clear that the signal amplitudes are well separated and restored by MCMC. Table 5.3 lists the mean-squared error of the restored amplitudes.

B. Experiment 2: Narrowband Scenario

In this experiment, we apply the algorithm to a narrowband scenario, where we reduce the bandwidth of the signals from 300 Hz to only 50 Hz. As in the previous experiment, we generate two Gaussian processes that are zero mean and variance, $\delta^2\sigma_w^2$, and bandlimited as follows

$$f \in [350, 400]\,\text{Hz}, \tag{93}$$

Parameter	True	Estimated	Relative Difference (%)
τ_0	$-7.5e^{-5}$	$-7.95e^{-5}$	6.00
τ_1	$7.5e^{-5}$	$7.25e^{-5}$	3.36
θ_0	-3.44	-3.65	6.00
θ_1	3.44	3.32	3.37

TABLE 5.2

Comparison between the true and estimated parameters.

Source 1	Source 2
-16.19 dB	-15.97 dB

TABLE 5.3

The MSE of the restored source amplitudes relative to the true signal amplitudes for experiment 1.

where the bandwidth of the signals is 50 Hz. Using the parameter values as given in Table 5.1, we can then generate $N = 50$ snapshots. In other words, by using the same data model developed in Section 2 and by tuning the bandwidth parameter Δf_k, one can model both narrowband and wideband scenarios. Fig. 9 exhibits the magnitude responses of the generated narrowband signals.

Fig. 10 is the histogram of the model order detection by the RJMCMC for the narrowband scenario. Figs. 11 and 12 depict the histogram and the trajectories of the estimation of the ISDs, respectively. As in the experiment for the wideband scenario, the algorithm runs for 10,000 iterations, and the chain centers very quickly around the true parameter values for the narrowband scenario as well. Table 5.4 summarizes a comparison between the true and estimated values of the incident angles and the corresponding ISDs. Furthermore, Fig. 13 exhibits a comparison between the restored and the true amplitudes. Table 5.5 lists the mean-squared error of the restored amplitudes for the narrowband case.

As seen in the simulations, the proposed method can perform joint detection, estimation and signal recovery for both narrowband and wideband scenarios. To date, there appears to be no previous method which accomplishes the same set of tasks. Therefore, performance comparisons with previous methods involves comparing the performance of only a subset of the capabilities of the proposed method with the respective criteria of previous methods. We present comparisions with the theoretical Cramér-Rao lower bound (CRLB) derived in [24] for this problem, and goodness-of-fit and efficiency tests [25]. We also present a comparison of the proposed method and the method of [10].

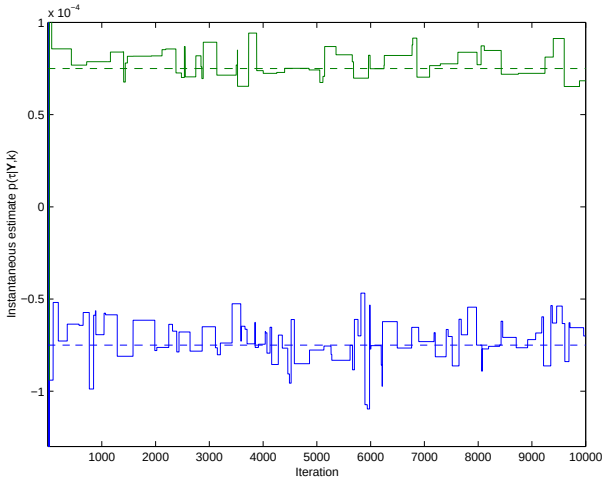

Fig. 6. Instantaneous estimate of the ISDs $\boldsymbol{\tau}$ for two sources: the solid lines are the estimates and the dashed lines are the true values.

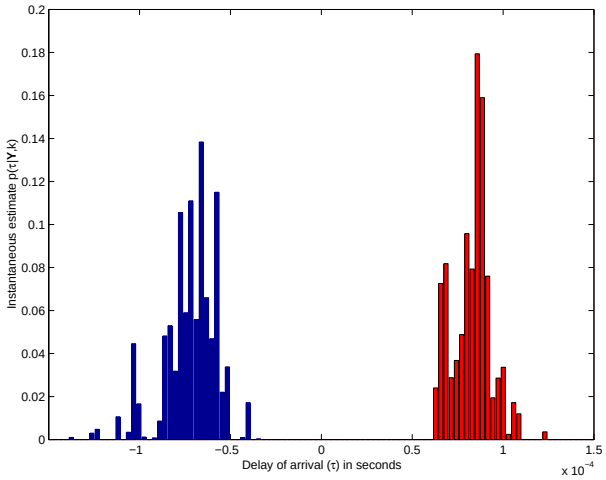

Fig. 7. Histogram of the ISDs of the sources after burn-in. The true values are $\pm 7.5 \times 10^{-5}$ seconds.

Parameter	True	Estimated	Relative Difference (%)
τ_0	$-7.5e^{-5}$	$-6.94e^{-5}$	7.47
τ_1	$7.5e^{-5}$	$8.13e^{-5}$	8.40
θ_0	-3.44	-3.18	7.56
θ_1	3.44	3.73	8.43

TABLE 5.4

Comparison between the true and estimated parameters for the narrowband scenario (Experiment 2).

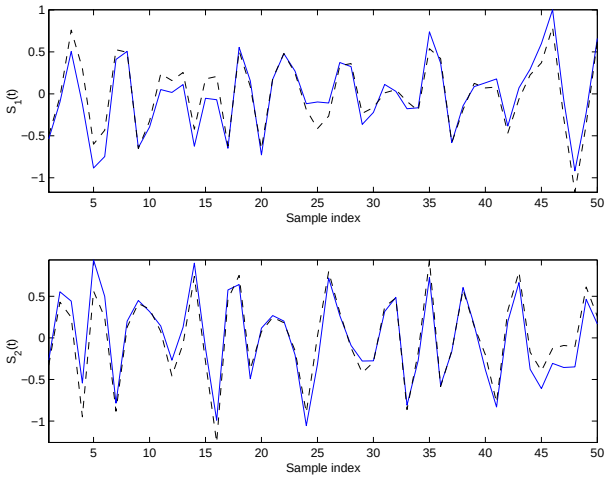

Fig. 8. A comparison between the true and the restored amplitudes using MCMC in one realization: solid lines correspond the restored amplitudes using MCMC and dashed lines correspond the true amplitudes.

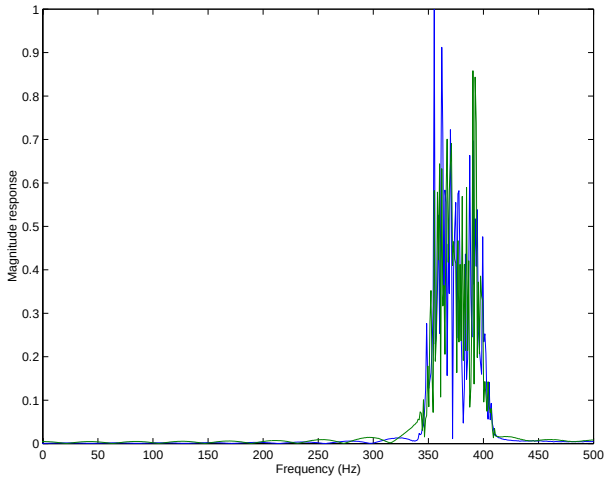

Fig. 9. The magnitude responses of the narrowband signals that are bandlimited within 350 and 400 Hz.

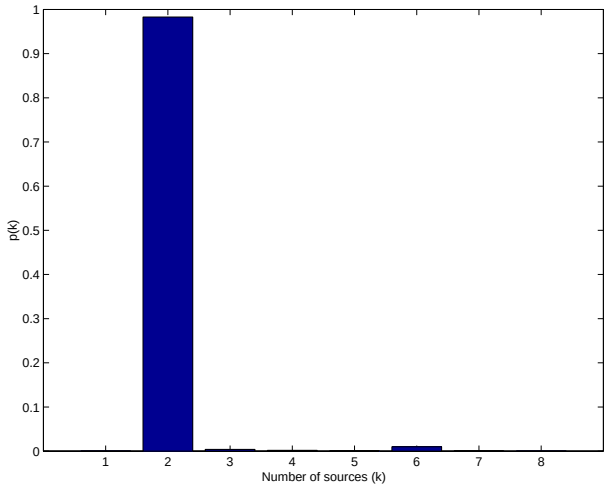

Fig. 10. Histogram of the number of sources after burn-in.

Source 1	Source 2
-17.31 dB	-17.76 dB

TABLE 5.5

THE MSE OF THE RESTORED SIGNALS RELATIVE TO THE TRUE SIGNAL AMPLITUDES FOR EXPERIMENT 2.

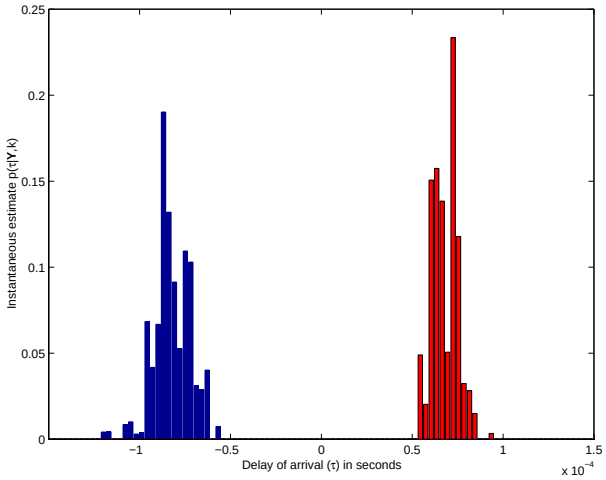

Fig. 11. Histogram of the ISDs of the sources after burn-in for the narrowband case.

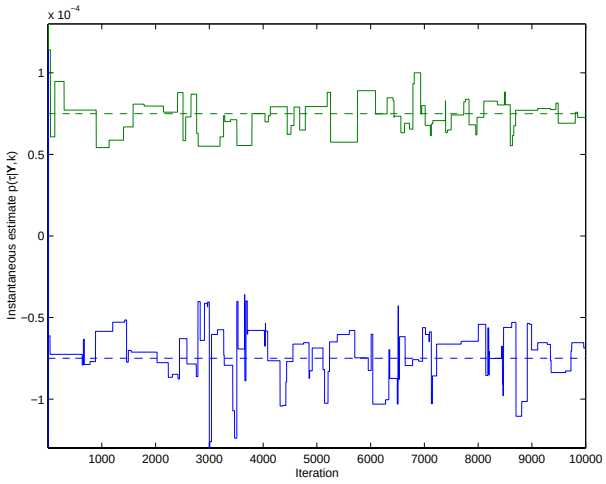

Fig. 12. Instantaneous estimate of the ISDs $\boldsymbol{\tau}$ for two sources for the narrowband case: the solid lines are the estimates and the dashed lines are the true values

Parameter	M	K	L	N	No. of MCMC iterations	σ_w^2	F_s (Hz)	$\boldsymbol{\tau}$ (seconds)
Value	8	2	8	50	$2,000$	0.0169	$1,000$	$[-0.5e^{-4} 0.5e^{-4}]$

TABLE 5.6

PARAMETERS FOR THE PERFORMANCE EVALUATION FOR THE PROPOSED METHOD.

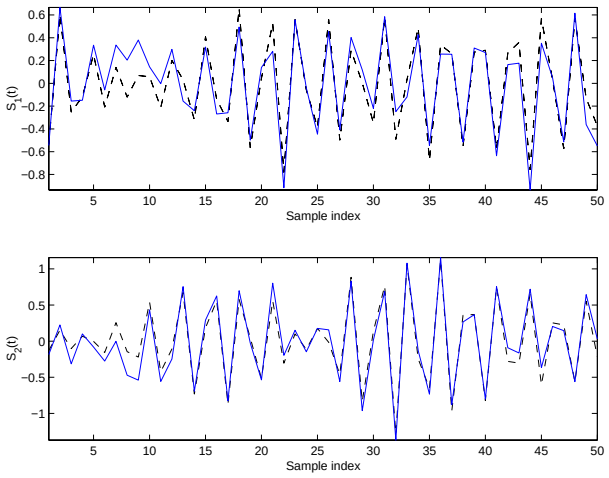

Fig. 13. A comparison between the true and the restored amplitudes using MCMC for one realization for the narrowband case: solid lines correspond the restored amplitudes using MCMC and dashed lines correspond the true amplitudes.

We now present the evaluation of the performance of the new method in terms of variances of the estimates of $\boldsymbol{\tau}$ as a function of SNR. This evaluation is obtained by applying the algorithm to 100 independent trials over a range of SNR, from -5dB to 18 dB. The remaining parameter values are given in Table 5.6.

The variances of the estimated $\boldsymbol{\tau}$ are plotted in Fig. 14 along with the respective theoretical CRLBs. As shown in Fig. 14, for SNR levels lower than -2dB, the algorithm starts to break down (i.e., departs rapidly from the CRLB. However, it is seen that the variances approach the CRLB closely, above this level. The reasons why the variances do not come closer to the theoretical CRLB are: 1) interpolation errors due to a non-ideal interpolation function being used and 2) the suboptimal procedure for estimating the source amplitudes. This procedure has an impact on the estimation accuracy of the DOA parameters. Further simulation results, as shown in Fig. 15, demonstrate that the probability of an error in detection of the model order tends to diminish toward zero with increasing number of snapshots, N, with moderate SNR values.

We also use the goodness-of-fit and efficiency tests [25] to evaluate the proposed method. Denote the normalized estimation error squared (NEES) for $\boldsymbol{\tau}$ by

$$\epsilon_{\boldsymbol{\tau}} \triangleq \tilde{\boldsymbol{\tau}}^T \boldsymbol{R}_{\tilde{\boldsymbol{\tau}}}^{-1} \tilde{\boldsymbol{\tau}}, \tag{94}$$

where

$$\tilde{\boldsymbol{\tau}} \triangleq \boldsymbol{\tau} - \hat{\boldsymbol{\tau}}, \tag{95}$$

$$\boldsymbol{R}_{\tilde{\boldsymbol{\tau}}} \triangleq E\left[\tilde{\boldsymbol{\tau}}\tilde{\boldsymbol{\tau}}^T\right]. \tag{96}$$

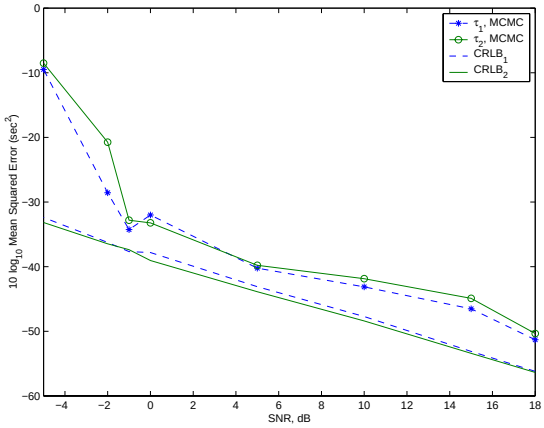

Fig. 14. Mean squared error of $\boldsymbol{\tau}$ versus the CRLB.

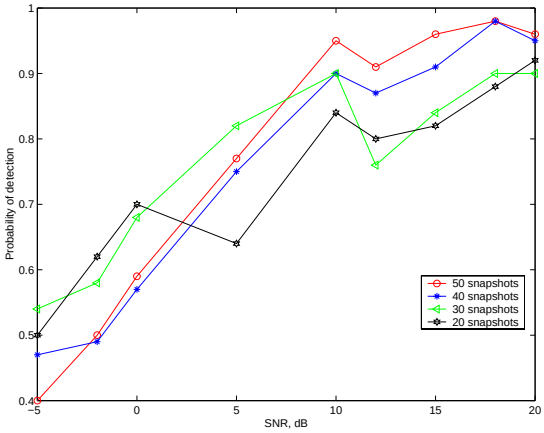

Fig. 15. Probability of detection as a function of number of snapshots for different SNR values.

The quantity $\epsilon_{\boldsymbol{\tau}}$ is chi-squared distributed with K degrees of freedom, that is

$$\epsilon_{\boldsymbol{\tau}} \sim \chi^2_K. \tag{97}$$

Given a confidence level, say 95%, a set of *g-sigma ellipsoids* for $\epsilon_{\boldsymbol{\tau}}$ [25] can be obtained with different SNR values. These ellipsoids can be used to evaluate how well the MCMC method is performing in estimating $\boldsymbol{\tau}$. Fig. 16 shows the impact of different SNR values on the estimation of $\boldsymbol{\tau}$ with a 95% confidence interval. It is clear that as SNR becomes large, the estimates concentrate more closely to the center of each ellipsoid, which corresponds to the true values of $\boldsymbol{\tau}$. However, as SNR falls below 0dB, it is found that the estimates distribute loosely around the center, as evident in Fig. 16. Accordingly, we can conclude that the proposed method would start to break down in estimating $\boldsymbol{\tau}$ when SNR is below 0dB under the conditions used for this set of experiments.

In addition, the proposed method was tested to determine whether it is an efficient estimator. Using the 95% confidence level, the two-sided probability region for the NEES [25] for $\boldsymbol{\tau}$ is

$$[\epsilon_1, \epsilon_2] = [1.6273, 2.4106]. \tag{98}$$

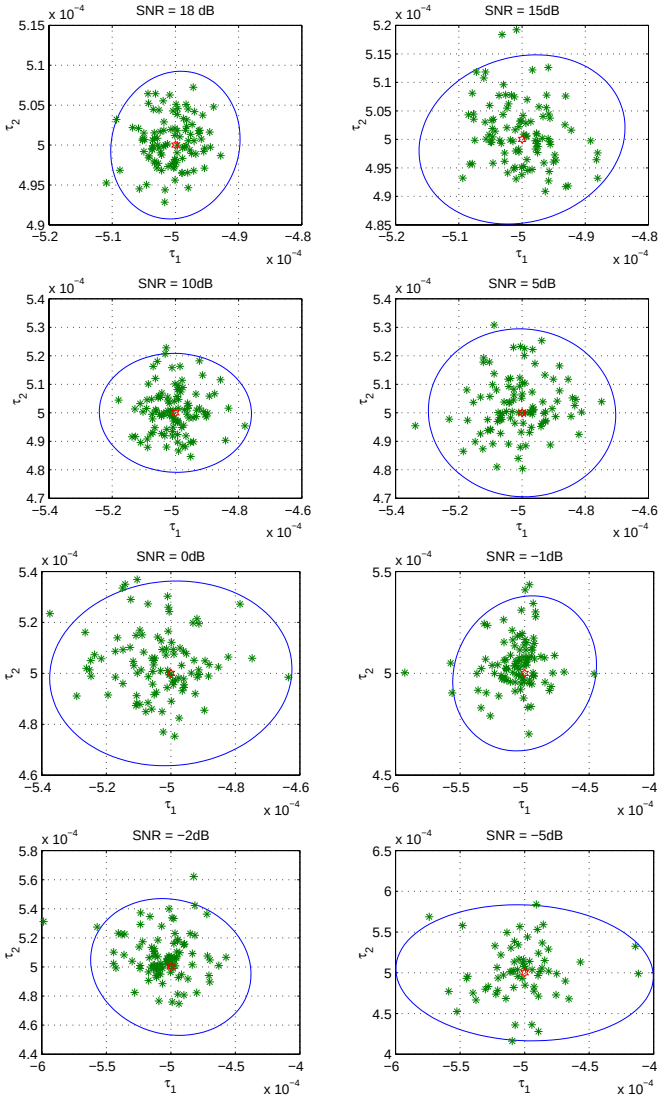

Fig. 16. The ellipsoids of the NEES with 95% confidence interval on MCMC with different SNR's: the triangle inside each ellipse corresponds the true value of $\boldsymbol{\tau}$, and the asterisks represent the distribution of the estimates of $\boldsymbol{\tau}$ of the 100 independent trials for a particular SNR.

Fig. 17 shows the NEES for $\epsilon_{\boldsymbol{\tau}}$ versus different SNR values. For SNR values above 0dB, the normalized errors fall inside the regions, that is, the method is consistent. However, as the SNR falls below 0dB, the errors are outside the bounds, indicating that the method starts with break down when the SNR is below 0dB. These findings are indeed consistent with those in Figs. 14 and 16.

Wideband array processing methods that rely on focusing [10] [11] require significantly more observations than the proposed method. Focusing methods require at least JM snapshots, where J is the number of frequency bins, so that full–rank covariance matrices can be formulated at each frequency, a requirement for DOA estimation. Since J is typically on the order of 32, a minimum of 256 snapshots would be required before DOA estimates could be produced using

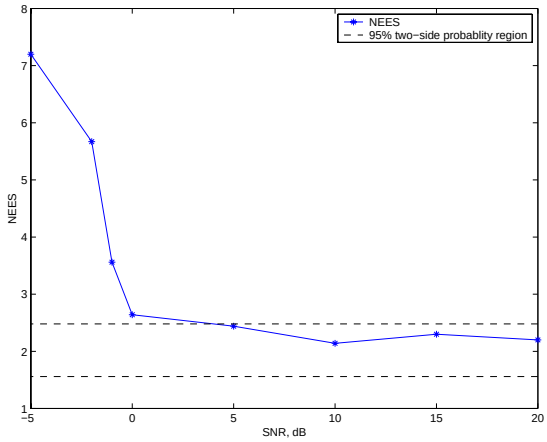

Fig. 17. Normalized estimation error squared from different SNR values with its 95% probability region.

the example of this section. Typically 10 times this number would normally be used, so that stable covariance matrix estimates would be obtained, yielding stable DOA estimates. As is seen in this section, DOA estimates that come close to the CRLB can be produced with less than 50 snapshots with the proposed method.

We now compare the performance between the proposed method and the TCT approach [10]. Table 5.7 lists the common parameters used in the comparison. 50 independent trials are run on each of these algorithms for different SNR values. The incident angles used are separated by a half-beamwidth. For the proposed method, 5,000 MCMC iterations are run for each simulation, whereas for the TCT algorithm, 32 frequency bins are used. Figure 18 depicts the variances of the TOA estimates obtained by these algorithms for different SNR values. According to Figure 18, the proposed method outperforms the TCT method throughout the range of SNR values shown. This can be explained by a few reasons. First, the TCT method requires sufficient data in each frequency bin so that a good estimate of the covariance matrix at that frequency can be determined. Therefore, when N is not large, the performance of the TCT method degrades. Second, at low SNR, the signal and noise subspace estimates, which are needed by the TCT method, degrade significantly at low SNR, giving rise to an early threshold.

Moreover, according to Figure 19, at low values of SNR and N, the performance of the MDL procedure, used by the TCT method for model order detection, degrades significantly. On the other hand, the proposed method, using a completely different detection approach, outperforms the TCT method under these conditions.

The MCMC method requires roughly $4-5$ times more computations than the TCT method, for a parameter set typical of that used here. The number of flop counts per each iteration of the MCMC method is

$$\text{flop counts}_{\text{MCMC}} \approx 2NM^2 + 2M^3 - 2N + LM \times [2k^2 + kL], \tag{99}$$

Parameter	M	K	N	$\boldsymbol{\theta}$ (degrees)
Value	8	2	320	$[3.67, 10.60]$

TABLE 5.7

PARAMETERS FOR THE PERFORMANCE COMPARISON BETWEEN THE PROPOSED METHOD AND THE TCT.

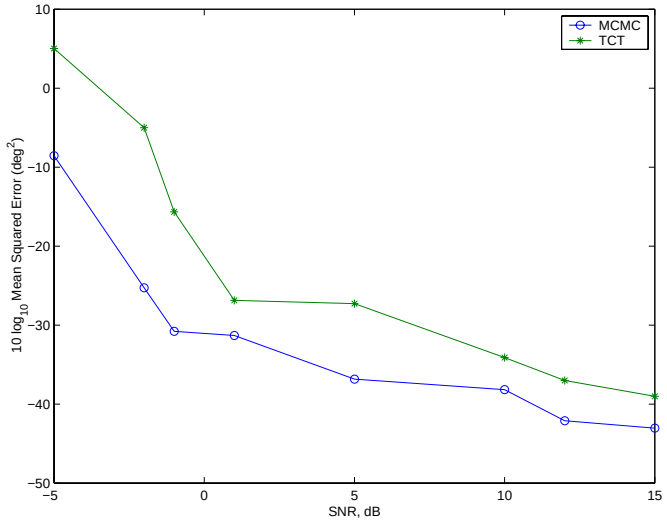

Fig. 18. Performance comparison between the proposed method and the TCT.

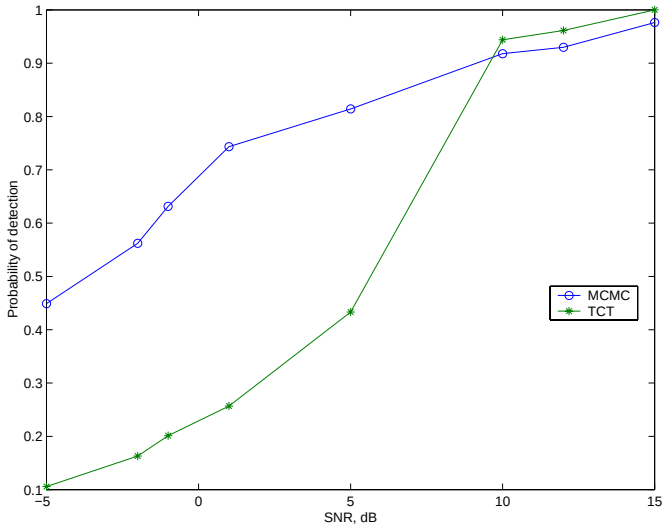

Fig. 19. Probability of detection obtained from the proposed method and the TCT as a function of SNR values.

and that of the TCT [14] is

$$\text{flop counts}_{\text{TCT}} \approx \tfrac{MN}{2}\log_2 M + 2NM^2 + [\tfrac{15}{2}J + 9]M^3. \quad (100)$$

This apparent disadvantage is mitigated by the fact that the MCMC algorithm provides estimation of the source waveforms, in conjunction with joint detection of model order and estimation of the DOA parameters. Substantially more computations would be required by the TCT method if the source amplitudes were also to be recovered. Further, the MCMC method is easily "parallelizable", thus offering the potential to considerably reduce computation times.

The source estimation procedure described in Section III-B is recursive. Under adverse conditions, the source estimates generated according to this procedure may occasionally become unstable, with very large error. As an example, when the SNR is 2dB, such a phenomenon appears with an approximate probability of 5%. However, when the SNR is -2dB, the probability grows to 22%. This problem may be alleviated by re–initializing the source amplitudes at periodic intervals throughout the observation interval.

VI. Conclusion

A novel structure for wideband array signal processing is proposed. It has been demonstrated the method applies equally well to the narrowband case. A Bayesian approach is used, where a posterior density function which has the nuisance parameters integrated out is formulated. The desired model order and DOA estimation parameters are determined through a reversible jump MCMC procedure. The source amplitudes are given using a MAP estimate. Simulation results support the effectiveness of the method, and demonstrate reliable detection of the number of sources and estimation of their times of arrival in white noise environment with a single linear array. As a result, the source signals are reliably restored. It has been demonstrated that the method requires only real arithmetic, and that significantly fewer observations are needed relative to what is required for focussing methods.

References

[1] D. Johnson, "The application of spectral estimation to bearing estimation problem," *Proceedings of the IEEE*, vol. 70, pp. 1018–1028, Sept. 1982.

[2] B. D. V. Veen and K. M. Buckley, "Beamforming: A Versatile Approach to Spatial Filtering," in *IEEE ASSP MAGAZINE*, Apr. 1988.

[3] R. Schmidt, "Multiple emitter location and signal parameter estimation," *IEEE Transactions on Antennas and Propagation*, vol. 34, pp. 284–280, Mar. 1986.

[4] C. Andrieu and A. Doucet, "Joint Bayesian model selection and estimation of noisy sinusoids via reversible jump MCMC," *IEEE Transactions on Signal Processing*, vol. 47, pp. 2667–2676, Oct. 1999.

[5] Q. Wu and D. Fuhrmann, "A parametric method for determining the number of signals in narrow-band direction finding," *IEEE Transactions on Acoustics, Speech, and Signal Processing*, vol. 39, pp. 1848–1857, Aug. 1991.

[6] S. Haykin and J. Reilly, "Maximum likelihood receiver for low-angle tracking radar; Part I: The symmetric case," *IEE Proceedings*, vol. 129 Pt.F, pp. 261–272, Aug. 1982.

[7] J. Reilly and S. Haykin, "Maximum likelihood receiver for low-angle tracking radar; Part II: The nonsymmetric case," *IEE Proceedings*, vol. 129 Pt.F, pp. 2667–2676, Oct. 1982.

[8] M. Wax, T. Shan, and T. Kailath, "Spatio-temporal spectral analysis by eigenstructure methods," *IEEE Transactions on Acoustics, Speech, and Signal Processing*, vol. 32, pp. 817–827, Aug. 1984.

[9] S. Valaee and P. Kabal, "A unitary transformation algorithm for wideband array processing," *Proc. Sixth IEEE SP Workshop on Statistical Signal & Array Processing (Victoria, BC)*, pp. 300–303, Oct. 1992.

[10] S. Valaee and P. Kabal, "Wideband array processing using a two-sided correlation transformation," *IEEE Transactions On Signal Processing*, vol. 44, pp. 160–172, Jan. 1995.

[11] H. Wang and M. Kaveh, "Coherent signal-subspace processing for the detection and estimation of angles of arrival of multiple wide-band sources," *IEEE Transactions on Acoustics, Speech, and Signal Processing*, vol. 33, pp. 823–831, Aug. 1985.

[12] H. Hung and M. Kaveh, "Focusing matrices for coherent signal-subspace processing," *IEEE Transactions on Acoustics, Speech, and Signal Processing*, vol. 36, pp. 1272–1281, Aug. 1988.

[13] M. Wax and T. Kailath, "Detection of signals by information theoretic criteria," *IEEE Transactions on Acoustics, Speech and Signal Processing*, vol. 33, pp. 387–392, Apr. 1985.

[14] S. Valaee, B. Champagne, and P. Kabal, "Localization of wideband signals using least-squares and total least-squares approaches," *IEEE Transactions On Signal Processing*, vol. 47, pp. 1213–1222, May 1999.

[15] K. Buckley and L. Griffiths, "Broadband signal subspace spatial spectrum (bass-ale) estimation," *IEEE Trans Acoust., Speech and Signal Processing*, vol. 36, pp. 953–964, July 1988.

[16] J. Krolik and D. Swingler, "Multiple broad-band source location using steered covariance matrices," *IEEE Trans Acoust., Speech and Signal Processing*, vol. 37, pp. 1481–1494, Oct. 1989.

[17] C. P. Robert and G. Casella, *Monte Carlo Statistical Methods*. New York: Springer Verlag, 1999.

[18] C. Andrieu, P. Djuric, and A. Doucet, "Model selection by MCMC computation," *Signal Processing*, vol. 81, pp. 19–37, Jan. 2001.

[19] W. Gilks, S. Richardson, and D. Spiegelhalter, *Markov Chain Monte Carlo in Practice*. New York: Chapman and Hall, 1998.

[20] P. Green, "Reversible jump Markov Chain Monte Carlo computation and Bayesian model determination," in *Biometrika*, vol. 82, pp. 711–732, 1995.

[21] G. H. Golub and C. F. V. Loan, *MATRIX Computations, 2nd Edition*. Baltimore, Maryland: The Johns Hopkins University Press, 1993.

[22] W. Hastings, "Monte Carlo sampling methods using Markov chains and their applications," in *Biometrika*, vol. 57, pp. 97–109, 1970.

[23] S. Godsill, "On the relationship between MCMC model uncertainty methods," *J. Comp. Graph. Stats.*, vol. 10(2), 2001.

[24] W. Ng, J. P. Reilly, and T. Kirubarajan, "The derivation of the theoretical CRLB for array signal processing for wideband signal," May 2002. Please download the document at http://www.ece.mcmaster.ca/∼reilly.

[25] X.-R. Li, Y. Bar-Shalom, and T. Kirubarajan, *Estimation, Tracking and Navigation: Theory, Algorithms and Software*. New York: John Wiley & Sons, June, 2001.